Structural and vibrational behavior of $2H$-$NbSe_2$ at high pressures

Grace P. Chen [1], Elena Bykova [2,3], Maxim Bykov [2,4], Eric Edmund [2], Zi-Yu Cao [5,*], Xiao-Jia Chen [5], Jesse S. Smith [6], Stella Chariton [7], Vitali B. Prakapenka [7], and Alexander F. Goncharov [2,†]

[1] *Magnet Program, Poolesville High School, Poolesville, Maryland 20837, USA*
[2] *Earth and Planets Laboratory, Carnegie Institution for Science, Washington, DC 20015, USA*
[3] *Bayerisches Geoinstitut, University of Bayreuth, Universitätsstrasse 30, D-95447 Bayreuth, Germany*
[4] *Institute of Inorganic Chemistry, University of Cologne, Greinstrasse 6, 50939 Cologne, Germany*
[5] *Center for High Pressure Science and Technology Advanced Research, Shanghai 201203, China*
[6] *HPCAT, X-ray Science Division, Argonne National Laboratory, Argonne, Illinois 60439, USA*
[7] *Center for Advanced Radiation Sources, The University of Chicago, Chicago, Illinois 60637, USA*

(Received 4 April 2022; accepted 15 June 2022; published 27 June 2022)

The high-pressure structural and vibrational properties of a layered transition metal dichalcogenide $2H$-$NbSe_2$ were investigated using single-crystal x-ray diffraction and Raman spectroscopy, demonstrating its structural stability up to 35 GPa. The lattice compressibility changes character from being highly anisotropic at low pressures to largely isotropic at high pressures. Concomitantly, the interatomic bonds demonstrate highly anisotropic compression behavior with the Se-Se interlayer bonds compressing by >20%, while the intramolecular Se-Se distance shows a nonmonotonic pressure dependence with a maximum at ∼12 GPa. The nearest-neighbor central force lattice vibrational model yields pressure dependencies of the interatomic forces in qualitative agreement with bond length compression, providing insight into the vibrational properties of $2H$-$NbSe_2$ at high pressures.

DOI: 10.1103/PhysRevB.105.224114

I. INTRODUCTION

$NbSe_2$ is a layered transition metal dichalcogenide (TMD) of the general formula MX_2. These compounds consist of triple X-M-X layers and crystallize in a variety of anisotropic structures, which differ by the layer stacking and layer structure. $NbSe_2$, which crystallizes in a hexagonal polytype with two layers in the unit cell ($2H$-$NbSe_2$), is prototypic for the occurrence of charge density waves (CDWs) which has been discovered in several TMDs [1]. The CDW in $2H$-$NbSe_2$ is found to be associated with the softening of the longitudinal acoustic phonon when temperature is below $T_{CDW} = 33$ K [2]. This makes detailed investigations of vibrational properties highly relevant for this system.

Pressure tuning of the electronic and vibrational properties represents a clean way to investigate the associated effects. It has been found that T_{CDW} drops down with pressure with an increasing pace [3], and it becomes suppressed >4.6 GPa [4]. Concomitantly, superconductivity which coexists and is expected to compete with CDW increases the critical temperature T_c from 7.2 K at ambient pressure until T_{CDW} and T_c cross ∼3.6 GPa at 8.2 K. At higher pressures, T_c continues to increase [5,6] with a smaller rate demonstrating a shallow maximum at 10.5 GPa and 8.5 K [6], which is much higher than the pressure for the T_{CDW} suppression; superconductivity persists to at least 19 GPa. A strong phonon anomaly at low temperatures also continues to at least 16 GPa, much higher than the collapsing CDW state [7]. Overall, the investigations show that the interplay among the electronic structure, vibrational dynamics, and superconductivity is more complex than previously thought, which calls for further investigations.

The structure and elastic properties of TMD are highly anisotropic, demonstrating easy interlayer cleavage and much stronger compressibility perpendicular to the layers than that parallel to the layers due to a difference in strength between intralayer van der Waals and interlayer covalent bonds [8,9]. It is remarkable that the CDW state persists in the limit of a single layer and even reveals superconductivity [10], making these compounds promising candidates for nanoscience applications. The highly anisotropic layered structure of TMD is an important ingredient for superconductivity, and it sets the stage for the Fermi surfaces with complex topology, which results in two-gap high-temperature superconductivity [11,12]. Application of pressure effectively tunes the lattice anisotropy, changing the topology of the Fermi surface, thus allowing us to follow the linked phenomena in detail.

Here, we report combined single-crystal x-ray diffraction (SCXRD) and Raman spectroscopy measurements examining the interatomic bond behavior under compression. We find that, by applying compression beyond 10 GPa to $2H$-$NbSe_2$, the elastic and vibrational properties become much less anisotropic, profoundly affecting the electronic structure and thus the phenomena of interest.

II. EXPERIMENTAL DETAILS

The experiments reported here were performed in a BX-90 diamond anvil cell [13] with Boehler-Almax diamond anvils and seats [14], using Ne as a pressure medium. A high-quality $2H$-$NbSe_2$ single crystal was purchased from HQGraphene.

*Present address: Center for Quantum Materials and Superconductivity (CQMS) and Department of Physics, Sungkyunkwan University, Suwon 16419, Republic of Korea.
†agoncharov@carnegiescience.edu

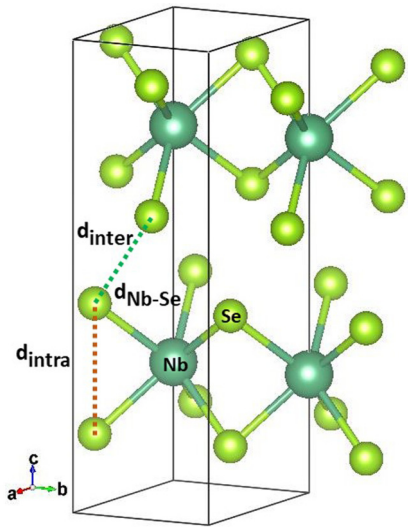

FIG. 1. Crystal structure of $2H$-$NbSe_2$. The bonds between the nearest-neighbor atoms are labeled.

Small flakes of $30 \times 60 \times 5\,\mu m^3$ sizes were chipped manually and loaded in a high-pressure cavity formed in a hole in a rhenium gasket pre-indented to a 35 μm thickness. Our SCXRD and Raman instrumentation has been described in previous publications (e.g., Ref. [15]). SCXRD measurements were performed in two runs at GeoSoilEnviroCARS (GSECARS) and HPCAT beamlines (sectors 13 and 16 of APS, ANL, respectively). The x-ray wavelengths were 0.3344 and 0.3445 Å, respectively. Raman spectra were measured in the beginning and at the end of these runs at GSECARS offline system [16] using the excitation wavelength $\lambda = 532$ nm and separately in the Earth and Planets Laboratory (EPL) of Carnegie Institution for Science and in the Center for High Pressure Science and Technology Advanced Research (HPSTAR), Shanghai ($\lambda = 488$ nm). Pressure was determined using the equation of state (EOS) of Ne in XRD and ruby fluorescence in the Raman experiment with an estimated uncertainty of ± 0.5 GPa. All experiments have been performed at room temperature.

III. RESULTS AND DISCUSSION

At ambient pressure, $2H$-$NbSe_2$ has a hexagonal $P6_3/mmc$ structure (Fig. 1) with two Se-Nb-Se trilayers with Nb in a trigonal prismatic coordination. Our SCXRD measurements show the stability of this $2H$-$NbSe_2$ structure at up to 35 GPa (Fig. 2, Table I, and Fig. S1 in the Supplemental Material [17]). This result agrees with a powder diffraction inves-

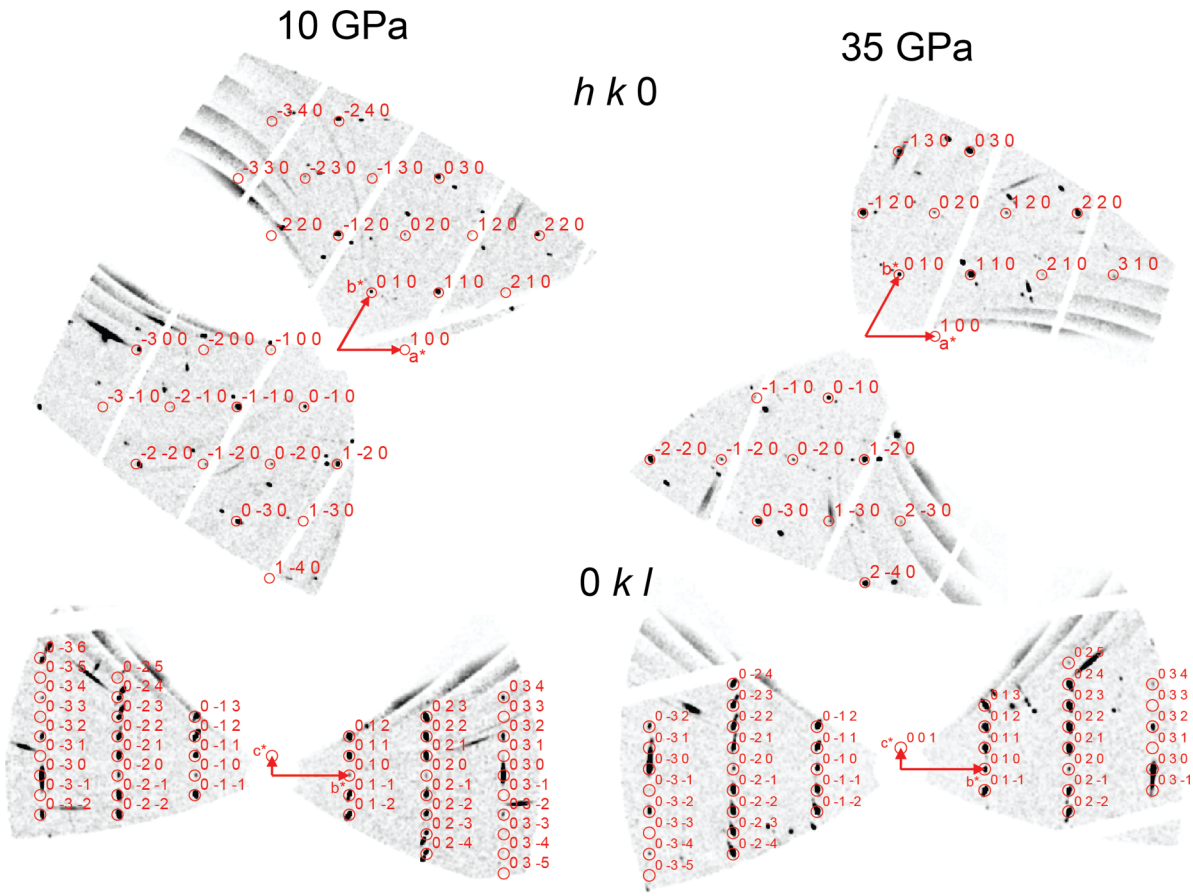

FIG. 2. Reconstructed reciprocal lattice plane of $NbSe_2$ at (a) 10.3(5) GPa and (b) 34.6(5) GPa obtained from single-crystal x-ray diffraction data. The x-ray wavelengths are 0.3344 Å (GSECARS) and 0.3445 Å (HPCAT), respectively. The observed diffraction spots have been indexed (circled) and used to determine the structure of $2H$-$NbSe_2$. Unindexed spots correspond to reflections from other crystallites; these could be observed because the grain size was close to the x-ray beam diameter.

TABLE I. Details of the crystal structure refinements for $2H$-$NbSe_2$ at high pressures.[a]

Pressure, GPa	2.5(5)	10.3(5)	18.0(5)	22.7(5)	27.4(5)	34.6(5)
a (Å)	3.4166(13)	3.3343(4)	3.274(2)	3.2583(17)	3.211(2)	3.1965(14)
c (Å)	12.180(14)	11.546(6)	11.308(9)	11.193(15)	11.04(4)	10.849(17)
V (Å^3)	123.13(17)	111.16(6)	104.98(15)	102.91(17)	98.6(4)	96.00(17)
ρ_{calc} (g/cm^3)	6.765	7.494	7.935	8.094	8.447	8.677
μ (mm^{-1}) absorption length	7.531	9.055	9.589	9.781	10.208	10.486
$2\Theta_{min}$ for data collection (°)	4.009	3.42	3.897	3.5	3.551	3.568
$2\Theta_{max}$ for data collection (°)	14.927	15.176	16.293	15.58	14.823	16.417
Completeness to $d = 0.8$ Å	0.494	0.554	0.7	0.633	0.5	0.618
Reflections collected	109	160	156	149	161	153
Independent reflections	51	49	67	57	43	52
Independent reflections $[I > 2\sigma(I)]$	47	43	53	51	34	47
Refined parameters	6	6	6	6	6	6
$R_{int}(F^2)$	0.0048	0.0553	0.0375	0.0213	0.0686	0.0227
$R(\sigma)$	0.0036	0.029	0.0432	0.018	0.0414	0.0163
R_1 $[I > 2\sigma(I)]$	0.0338	0.054	0.049	0.0541	0.0547	0.0529
wR_2 $[I > 2\sigma(I)]$	0.083	0.1358	0.1154	0.1569	0.12	0.1425
R_1	0.034	0.0591	0.0638	0.0568	0.0605	0.055
wR_2	0.0834	0.1402	0.1264	0.1616	0.1235	0.1446
Goodness of fit on F^2	1.223	1.285	1.068	1.236	1.086	1.383
$\Delta\rho_{max}$ (e/Å^3)	1	1.707	2.717	2.266	1.88	1.673
$\Delta\rho_{min}$ (e/Å^3)	−1.076	−1.664	−2.321	−2.225	−1.46	−2.626
z (Se1)	0.11230(7)	0.1045(3)	0.1016(2)	0.1002(4)	0.0984(3)	0.0975(3)
U_{eq} (Nb1) (Å^2) [b]	0.0136(9)	0.0114(12)	0.0084(7)	0.0134(11)	0.0170(12)	0.0157(12)
U_{iso} (Se1) (Å^2)	0.0131(12)	0.0136(15)	0.0085(7)	0.0142(10)	0.0192(14)	0.0156(11)
$d1$ (Nb1-Se1) (Å)	2.589(2)	2.555(2)	2.5279(19)	2.520(3)	2.498(5)	2.479(3)
$d2$ (Se1 … Se1) (Å)	3.373(3)	3.087(4)	2.975(3)	2.927(5)	2.856(7)	2.807(5)
Data collection	GSECARS	HPCAT	HPCAT	HPCAT	HPCAT	HPCAT

[a]Space group $P6_3/mmc$, $Z = 2$, Wyckoff positions of the atoms: Nb1 $2b$ (0,0,0.25), Se1 $4f$ (0.3333, 0.6667, z).
[b]U_{eq} is defined as one-third of the trace of the orthogonalized U_{ij} tensor.

tigation [9], where $P6_3/mmc$ structure was reported to be stable up to 39 GPa, but the atomic positions could not be determined. The results of our SCXRD analysis are summarized in Table I.

The lattice parameters contract with pressure anisotropically (Fig. 3), initially mostly along the c axis. The linear compressibilities extracted from the compression curves (Fig. 4) by fitting the data to the Vinet equations for the lattice parameters $P = B_0(1-\eta)\eta^{-2}\exp[1.5(B_1-1)(1-\eta)]$, where B_0 and B_1 are the inverse of the linear compressibilities and the derivative of this quantity with respect to pressure at 0 GPa, respectively, and $\eta = x/x_0$, where x and x_0 are the lattice parameters (a or c) under compression and at 0 GPa, respectively. The results show that the anisotropy rapidly diminishes with pressure [Fig. 4(a)], and $2H$-$NbSe_2$ compresses almost isotropically at the highest pressures examined here. Concomitantly, the c/a lattice parameter ratio drops drastically with pressure but becomes almost constant >10 GPa [inset to Fig. 4(a)]. The anisotropy in compressibility occurs because of the weak interlayer van der Waals bond (Fig. 1), which compresses the most, while the intralayer Se-Se distance changes very little, initially even slightly increasing and then decreasing after passing the maximum at ∼12 GPa [Fig. 4(b)]. The compression of the intralayer covalent Nb-Se bonds is steady and almost linear with pressure. The volume compression is smooth, and it can be presented well by a single Vinet EOS (Fig. S2 in the Supplemental Material [17]).

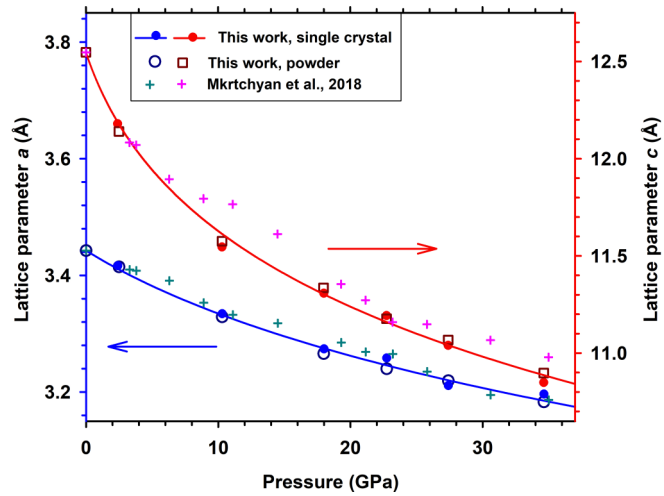

FIG. 3. The unit cell lattice parameters of $2H$-$NbSe_2$ deduced from single-crystal and powder x-ray diffraction data. Please note the different vertical axes (color coded) for the a and c lattice parameters. The error bars (Table I) for the lattice parameters are smaller than the symbol size. The solid lines are the best fits to the Vinet equations for the lattice parameters (see text) with the following parameters: $a_0 = 3.443(2)$; $B_0^a = 244(23)$ GPa; $B_1^a = 5.3(1.0)$; $c_0 = 12.547(8)$; $B_0^c = 62(6)$ GPa; $B_1^c = 6.8(5)$. Data from this paper are compared with those of Ref. [9].

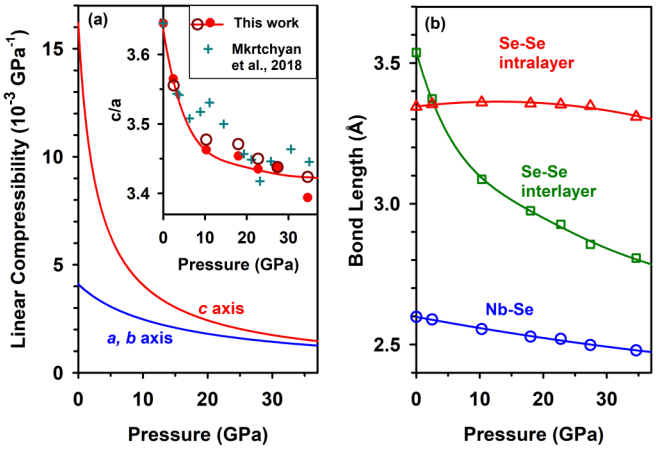

FIG. 4. (a) The linear compressibilities and (b) bond lengths vs pressure of $2H$-$NbSe_2$ derived from single-crystal (SC) and powder x-ray diffraction (XRD) measurements. The inset to (a) shows the pressure dependence of the c/a ratio (filled symbols: single crystal, open symbols: powder). Data from this paper are compared with those of Ref. [9].

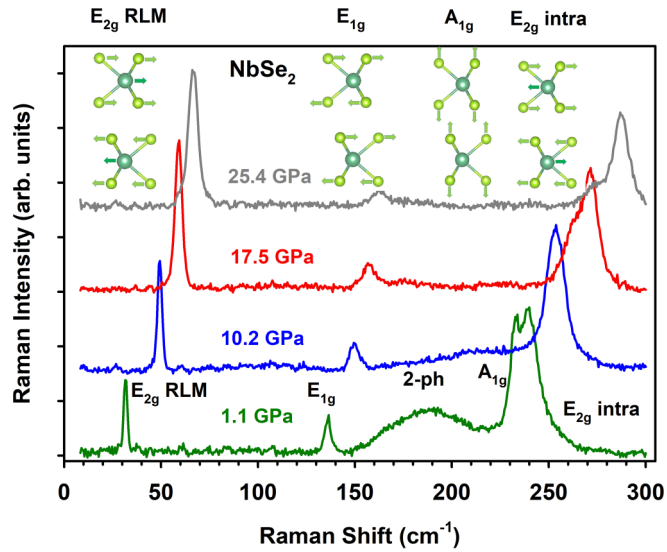

FIG. 5. Raman spectra of $2H$-$NbSe_2$ at elevated pressures measured at HPSTAR. The modes are assigned and labeled following the literature [18,19]. The atomic motions corresponding to the Raman active modes are shown in cartoons at the top. The excitation wavelength is 488 nm.

Raman spectroscopy has been used to probe the bond behavior upon compression. The Raman spectra of $2H$-$NbSe_2$ with 6 atoms in the unit cell, which consists of two layers, are predicted to display four modes: $A_{1g} + E_{1g} + 2E_{2g}$. The $A_{1g} + E_{1g}$ intralayer modes correspond to the opposite vibrations of Se atomic planes in the *ab* plane and along the *c* axis, respectively. The two E_{2g} modes are the in-plane vibrations of Se and Nb atomic planes, which yield a rigid layer mode (RLM) E^1_{2g} and an intralayer E^2_{2g} mode modulating the inter- and intramolecular bonds, respectively. In addition, a rather intense broad two-phonon (2-ph) scattering feature was previously observed [18,19].

Our Raman spectra show the expected modes and trace their behavior at high pressures (Figs. 5 and S3 in the Supplemental Material [17]). As pressure increases, all peaks shift to higher frequencies. The interlayer low-frequency E^1_{2g} mode demonstrates the largest relative frequency shift ($\beta = \frac{\delta\nu}{\nu_0 \delta P}$, where ν_0 is the Raman frequency at 0 GPa). The A_{1g} and E^2_{2g} intramolecular modes have very close frequencies at 0 GPa (A_{1g} : 231 cm^{-1} and E^2_{2g}: 238 cm^{-1} [18]); polarization measurements are needed to separate and assign these modes. The stressed diamond anvils rotate and scramble polarizations of the laser and the scattered signal beams, making it challenging to measure these two modes separately. Nevertheless, < 4 GPa, these modes are spectrally resolved; then only one peak can be observed between 4 and 13 GPa, while at higher pressures, the peak splits again, and this splitting increases with pressure. This behavior suggests the Raman mode crossing at $\sim$10 GPa, which is consistent with the pressure dependencies of their frequencies obtained by the high-frequency peak fitting to two modes (Fig. 6).

At low pressures, the spectra are dominated by the intralayer A_{1g} and E^2_{2g} modes, but the low-frequency E^1_{2g} gains intensity and dominates with the increase of pressure. In our experiments, we have also measured a weak E_{1g} mode up to 25 GPa, which decreases its intensity with pressure continuously. It is interesting that the 2-ph band decreases in intensity with pressure rather abruptly and becomes undetectable $>$15 GPa.

We explored the nearest-neighbor central force model previously used in Refs. [18,20], which we explicitly extended to include the interlayer coupling ε via the Se-Se interlayer atomic forces. The other interactions of the nearest-neighbor central force model are described by the intralayer Nb-Se force constant γ and the Se-Se bond intralayer force constant β. In terms of this model, the Raman frequencies can be determined as follows:

$$\omega^2_{E^1_{2g}} = \frac{3\varepsilon \sin^2\eta}{2m_2 + m_1},$$

$$\omega^2_{E_{1g}} = \frac{3(\varepsilon \sin^2\eta + \gamma \sin^2\theta)}{m_2},$$

$$\omega^2_{E^2_{2g}} = \frac{3(\varepsilon \sin^2\eta + \gamma \sin^2\theta)}{\mu},$$

$$\omega^2_{A_{1g}} = \frac{2\beta + 3\varepsilon \cos^2\eta + 3\gamma \cos^2\theta}{m_2},$$

where m_1 and m_2 are the atomic masses of Nb and Se, respectively, $\mu = 2\ m_1 m_2/(m_1 + 2m_2)$ is the reduced mass, and η and θ are the angles between the Se-Se and Nb-Se bonds and the crystal axis, respectively.

The interlayer force constant ε (Fig. 7) determined from the E^1_{2g} frequency and the Se-Se bond angle determined from our SCXRD data show a rapid increase with pressure followed by a gradual decrease in the pressure slope. The intralayer Nb-Se force constant γ can be obtained from the E^2_{2g} and E_{1g} mode frequencies and the Nb-Se bond angle: both these modes include the modulation of the bonds introduced with the γ and ε force constants (Fig. 5). We determined γ from the E_{1g} mode frequency to avoid some ambiguity in the E^2_{2g}

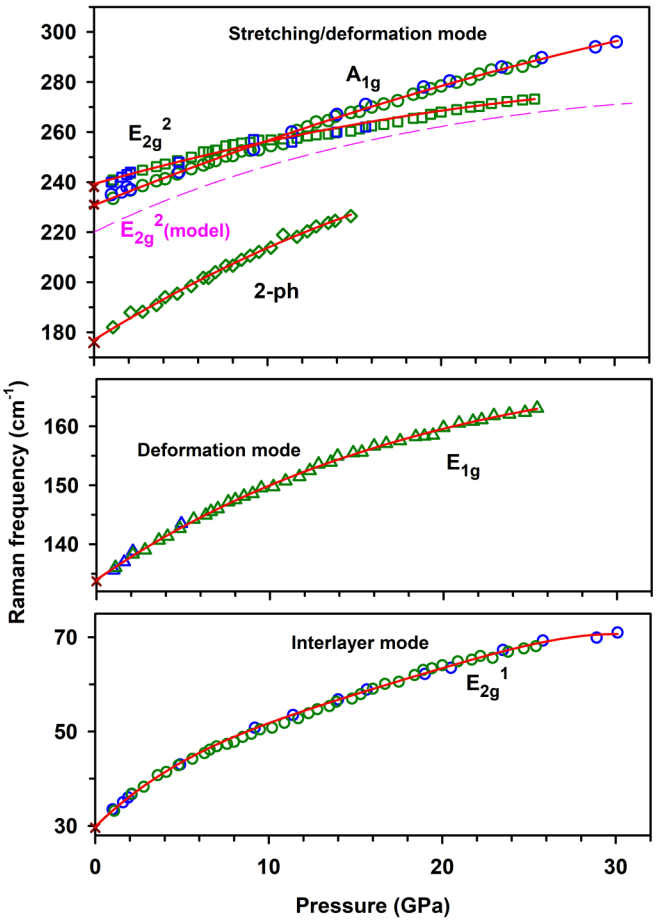

FIG. 6. Raman frequencies of $2H$-$NbSe_2$ at elevated pressures. Open symbols of different colors are data from this paper measured at EPL and HPSTAR (blue and green symbols, respectively). The error bars for the Raman frequencies are smaller than the symbol size. The pressure uncertainty is ±0.5 GPa. Solid lines are guides to the eye. Data at 0 GPa (x crosses) are from Ref. [18]. A dashed pink line shows the results of the nearest-neighbor central force model calculations of the E_{2g}^2 mode frequency (see text).

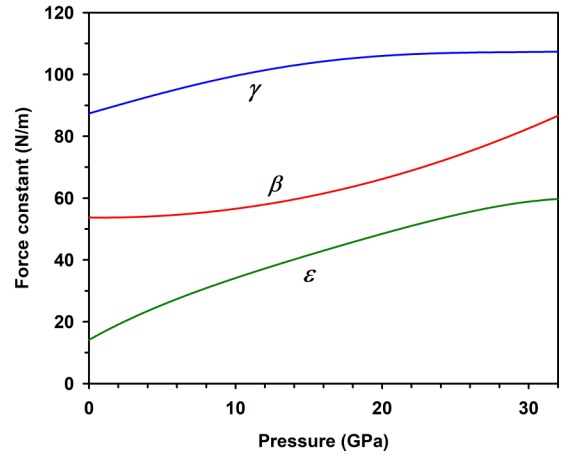

FIG. 7. Interatomic central force constants of $2H$-$NbSe_2$ at elevated pressures determined from the Raman frequencies.

mode frequency due to the A_{1g} and E_{2g}^2 mode crossing (Fig. 6). Finally, we determined the last parameter of the model, the Se-Se bond intralayer force constant β, from the A_{1g} mode frequency. The A_{1g} mode also involves the ε and γ force constants, which we have already determined. The E_{2g}^2 mode frequency is redundant in this procedure; we plotted it as a function of pressure in Fig. 6. The dependence determined from the model is slightly lower than the experimental one; the difference is well within 10%, demonstrating that this simple model works reasonably well.

The force constants determined here (Fig. 7) at high pressures agree reasonably well with those determined at ambient pressure [18], given that intermolecular coupling was neglected in this paper for the high-frequency modes. Our results show that pressure affects both inter- and intralayer force constants, shifting the balance between them. The interlayer coupling ε is being increased by >4 times at 32 GPa. This is consistent with ∼25% of contraction of the Se-Se interlayer bond lengths (Fig. 3). At the same time, the Se-Nb-Se layer thickness, which is equal to the intralayer Se-Se bond length, changes very little, decreasing only slightly at highest pressures. Accordingly, the Se-Se intralayer force constant β is pressure independent at the initial stage of compression and then increases at the highest pressures. The Nb-Se intralayer force constant γ increases steadily with pressure, but this tendency saturates at high pressures. This is consistent with a steady contraction of the Nb-Se bond length (Fig. 3). All force constants become comparable in value at high pressures. In this regime, $2H$-$NbSe_2$ transforms to a three-dimensional (3D) solid. This is consistent with a close-to-isotropic compression character determined here (Fig. 3).

This transformation in the interatomic force field also results in a change in dispersion curves, confirmed by the behavior of the 2-ph band (Fig. 4). This peak corresponds to the overtone of a flat part of the longitudinal optical phonon branch in the Γ-M direction of the Brillouin zone [7], which contributes greatly in the density of the phonon states and, thus, in the 2-ph Raman scattering processes. These modes contribute to the Eliashberg function $\alpha^2F(\omega)$, yielding a low-frequency peak in the electron-phonon coupling function [7]. Our observations show a decrease in intensity of the 2-ph band, suggesting that the dispersion curve along the Γ-M direction of the Brillouin zone changes, likely becoming more regular.

The results of this paper can be used for building more accurate vibrational mode models and for benchmarking the behavior of $NbSe_2$ to higher pressures, where the $2H$ layer structure transforms to a 3D structure. These results in the limit of low pressure can be used to address low-temperature superconducting and CDW order competitions related to the Fermi surface topology. In the limit of high pressures, our data suggest that the phonon dispersion curves become more regular, changing the electron-phonon interaction strength—the result which sheds light on the pressure dependence of the superconducting temperature T_c at high pressures.

ACKNOWLEDGMENTS

G.P.C. acknowledges the internship program at Carnegie Institution for Science. Parts of this paper were carried out at

the GSECARS (The University of Chicago, Sector 13), Advanced Photon Source (APS), Argonne National Laboratory. GSECARS is supported by the National Science Foundation (NSF)—Earth Sciences (No. EAR-1634415). Use of the GSECARS Raman System was supported by the NSF MRI Proposal (No. EAR-1531583). Portions of this paper were performed at HPCAT (sector 16) of the APS, Argonne National Laboratory. HPCAT operations are supported by U.S. Department of Energy (DOE) National Nuclear Security Administration's Office of Experimental Sciences. The APS is a DOE Office of Science User Facility operated for the DOE Office of Science by Argonne National Laboratory under Contract No. DE-AC02-06CH11357. M.B. acknowledges the support of Deutsche Forschungsgemeinschaft (DFG Project No. BY112/2-1). E.B., M.B., and A.F.G. acknowledge the support of the Carnegie Institution for Science.

[1] J. A. Wilson, F. J. Di Salvo, and S. Mahajan, Adv. Phys. **24**, 117 (1975).
[2] F. Weber, S. Rosenkranz, J. P. Castellan, R. Osborn, R. Hott, R. Heid, K. P. Bohnen, T. Egami, A. H. Said, and D. Reznik, Phys. Rev. Lett. **107**, 107403 (2011).
[3] C. Berthier, P. Molinié, and D. Jérome, Solid State Commun. **18**, 1393 (1976).
[4] Y. Feng, J. Wang, R. Jaramillo, J. v. Wezel, S. Haravifard, G. Srajer, Y. Liu, Z.-A. Xu, P. B. Littlewood, and T. F. Rosenbaum, Proc. Natl. Acad. Sci. USA **109**, 7224 (2012).
[5] O. Moulding, I. Osmond, F. Flicker, T. Muramatsu, and S. Friedemann, Phys. Rev. Res. **2**, 043392 (2020).
[6] H. Suderow, V. G. Tissen, J. P. Brison, J. L. Martínez, and S. Vieira, Phys. Rev. Lett. **95**, 117006 (2005).
[7] M. Leroux, I. Errea, M. Le Tacon, S.-M. Souliou, G. Garbarino, L. Cario, A. Bosak, F. Mauri, M. Calandra, and P. Rodière, Phys. Rev. B **92**, 140303(R) (2015).
[8] Z.-H. Chi, X.-M. Zhao, H. Zhang, A. F. Goncharov, S. S. Lobanov, T. Kagayama, M. Sakata, and X.-J. Chen, Phys. Rev. Lett. **113**, 036802 (2014).
[9] V. Mkrtchyan, R. Kumar, M. White, H. Yanxon, and A. Cornelius, Chem. Phys. Lett. **692**, 249 (2018).
[10] M. M. Ugeda, A. J. Bradley, Y. Zhang, S. Onishi, Y. Chen, W. Ruan, C. Ojeda-Aristizabal, H. Ryu, M. T. Edmonds, H.-Z. Tsai *et al.*, Nat. Phys. **12**, 92 (2016).
[11] T. Dahm and N. Schopohl, Phys. Rev. Lett. **91**, 017001 (2003).
[12] J. G. Rodrigo and S. Vieira, Physica C **404**, 306 (2004).
[13] I. Kantor, V. Prakapenka, A. Kantor, P. Dera, A. Kurnosov, S. Sinogeikin, N. Dubrovinskaia, and L. Dubrovinsky, Rev. Sci. Instrum. **83**, 125102 (2012).
[14] R. Boehler and K. De Hantsetters, High Pressure Res. **24**, 391 (2004).
[15] M. Bykov, E. Bykova, C. J. Pickard, M. Martinez-Canales, K. Glazyrin, J. S. Smith, and A. F. Goncharov, Phys. Rev. B **104**, 184105 (2021).
[16] N. Holtgrewe, E. Greenberg, C. Prescher, V. B. Prakapenka, and A. F. Goncharov, High Pressure Res. **39**, 457 (2019).
[17] See Supplemental Material at http://link.aps.org/supplemental/10.1103/PhysRevB.105.224114 for Figs. S1–S3.
[18] C. S. Wang and J. M. Chen, Solid State Commun. **14**, 1145 (1974).
[19] H. M. Hill, A. F. Rigosi, S. Krylyuk, J. Tian, N. V. Nguyen, A. V. Davydov, D. B. Newell, and A. R. Hight Walker, Phys. Rev. B **98**, 165109 (2018).
[20] R. A. Bromley, Philos. Mag. **23**, 1417 (1971).